Proc. Natl. Acad. Sci., India, Sect. A Phys. Sci. (April–June 2014) 84(2):281–295
DOI 10.1007/s40010-014-0143-7

RESEARCH ARTICLE

Quantitative Analysis of Intermolecular Interactions in 7-Hydroxy-4-methyl-2*H*-chromen-2-one and Its Hydrate

Piyush Panini · K. N. Venugopala · B. Odhav · Deepak Chopra

Published online: 9 March 2014

Abstract The determination of the crystal and molecular structure of organic compounds has contributed immensely towards the area of crystal engineering. This contributes towards the understanding of the molecular geometry and the different intermolecular interactions which control crystal packing. An approach which quantifies the energetics associated with the formation of different "molecular pairs" is of importance to recognize the hierarchy of intermolecular interactions present in the crystal. We intend to explore different computational tools which contribute towards the field of crystal engineering. In this regard, the crystal structure of 7-hydroxy-4-methyl-2*H*-chromen-2-one and its hydrate were re-determined and their crystal packing were analyzed in terms of the interaction energy of different intermolecular interactions, calculated by PIXEL method, contributing towards the stabilization of the crystal packing. The system is so chosen such that it allows the analysis of weak interactions like C–H···O, C–H···π, π···π, *lp*···π etc. in the presence of strong O–H···O hydrogen bonds and also allows for a systematic exploration of the effect of solvent (water in the present case) on the crystal packing. The calculation of the lattice energy reveals that the anhydrous form is 7 kcal/mol more stable than the corresponding hydrate. The major stabilization towards the crystal packing were observed to come from strong O–H···O=C hydrogen bonds (9 kcal/mol) in case of the anhydrous form while in case of its hydrate, water acts as both an acceptor and a donor of the hydrogen bonds, the interaction energy ranging from 5 to 9 kcal/mol. The weak C–H···O hydrogen bond were found to be the second highest contributor (I.E = 3.5–5.5 kcal/mol) towards the stabilization of the packing in both the crystal structures. The main differences in the crystal packing were observed in the presence of weaker interactions in their crystal packing. The weak C–H···π, O(*lp*)···C=O interactions were observed in the crystal packing of the anhydrous form while the π···π, O(*lp*)···π interactions stabilize the crystal packing in case of its hydrate. This phenomenon were further well supported by the analysis of the Hirshfeld surfaces mapped with different properties, 2D-fingerprint plots, electrostatic potential mapped on the Hirshfeld surface and electron density isosurface (calculated by ab initio calculation at DFT-D3/B97-D) at both solid state and optimized geometry.

Keywords Coumarin · Hirshfeld · PIXEL · Molecular pairs · Intermolecular interactions

P. Panini · D. Chopra (✉)
Department of Chemistry, Indian Institute of Science Education and Research Bhopal, Indore By-pass Road, Bhauri, Bhopal 462066, Madhya Pradesh, India
e-mail: dchopra@iiserb.ac.in

K. N. Venugopala · B. Odhav
Department of Biotechnology and Food Technology, Durban University of Technology, Durban 4001, South Africa

Introduction

Coumarin derivatives are found to exhibit a wide range of biological activities such as anticoagulant, anti-inflammatory, anti-carcinogenic, antioxidant and antibiotic activities [1–6]. It is used as an inhibitor for protein tyrosine phosphatase 1B, acetyl cholinesterase and monoamine oxidase [7–9]. In addition, the 2*H*-chromen-2-one derivatives have also received attention in the area of dye and pigment industries as it is useful in the production of fluorescent materials [10]. The related derivatives of these class of compounds are also widely explored in the area of

crystal engineering as these allows the possibility to analyse the role and influence of weaker interactions such as C–H···O, C–H···π, π···π stacking etc. in the presence of strong O–H···O hydrogen bonds [11–13]. The crystal formation is the periodic three dimensional self-assembling processes in molecules. This is a spontaneous process and proceeds through a series of molecular recognition events. The phenomenon of the molecular recognition process may be considered to be driven or stabilized by the mutual interactions which can be either strong or weak present between them during such a process. A co-operative interplay of various intermolecular interactions during the molecular recognition process may also lead to formation of different solid forms of the compound [14]. This phenomenon is popularly known as polymorphism and may lead to changes in various physical and chemical properties of the compound such as melting point, particle size, stability, tableting, bioavailability, dissolution rates and pharmacological activity [15].The crystal structure prediction of a given molecule or set of molecules (cocrystals or salt or solvates) [16, 17] and the design of a material with desirable properties are also very important and an emerging field in the area of crystal engineering [18]. Therefore the systematic but extensive study of the nature of interactions which influence the process of crystal formation has now become very important and of significance in the area of crystal engineering. In this regard, the strong hydrogen bonds e.g. O/N–H···O/N [19] and relatively weaker hydrogen bonds C–H···O/N [20] are now very well studied and considered to be most reliable forces for the recognition of molecules in the solid state. The focus is now shifted towards the utilization of weaker forces such as π···π [21–24] and *lp*···π [25–29] interactions in the formation of the crystal. In recent times, weak interactions like π···π, *lp*···π have become significantly important in the area of chemistry and biology [21–29]. In the view of all the above-mentioned concepts, not only qualitative (based only on the geometrical distance-angle criteria) but the quantitative evaluation of these interactions is now a prerequisite to enable an improved understanding of the nature of different intermolecular interactions [30–32]. Many computational tools have significantly contributed in this regard. For example (1) the PIXEL method [33, 34] which is based on empirical partitioning of the interaction energy or cohesive energy into their Coulombic, polarization, dispersion and repulsion contribution, provide important insights towards the crystal packing contributions for the calculation of lattice energy [35, 36] (2) the analysis of the Hirshfeld surfaces [37] and the associated 2D-fingerprint plots [38] which provide useful visualization tool for the analysis of intermolecular interactions and the crystal packing behaviour of molecules in the crystal.

In this work, the compound 7-hydroxy-4-methyl-2*H*-chromen-2-one were selected for such a study because it allows the for the formation of various weaker interactions such as π···π and *lp*···π in the presence of strong O–H···O hydrogen bonds and relatively weaker C–H···O hydrogen bonds. The crystallization experiments (experimental section) in this work also resulted in the formation of a hydrate of the title compound. The formation of the hydrate also has a profound influence on the crystal packing of the compound relative to that of the anhydrous form.

In this present study, we have undertaken quantitative crystal packing analysis for the of a Coumarin derivative (7-hydroxy-4-methyl-2*H*-chromen-2-one) and its hydrate. The main focus of this study involves a detailed investigation of the nature of weak interactions, namely π···π and *lp*···π with detail inputs from lattice energy and intermolecular interaction calculations (with total energy being partitioned into their Coulombic, polarization, dispersion and repulsion contributions). In addition, Hirshfeld surfaces and associated 2D-fingerprint plots along with the associated electrostatic potential [39] map provide detail information about patterns of chemical reactivity in this molecule.

Experimental Section

In order to isolate more than one solid state form (the phenomenon of polymorphism) of the biologically active compound 7-hydroxy-4-methyl-2*H*-chromen-2-one, the single crystals of the purified solid [40] were grown from different solvents [dichloromethane + hexane, tetrahydrofuran, chloroform, acetone, acetonitrile, ethyl acetate, 2-propanol] at room temperature. The crystals obtained from all the possible crystallizations were checked for the presence of polymorphism. The crystal structure for the anhydrous [41] (**CHRM**) and the hydrate [42] (**CHRM·H$_2$O**) have been reported previously but we have again synthesised, purified and recrystallized the compounds and re-determined the crystal structure (Table 1). The obtained solid forms were analyzed by differential scanning calorimeter (with Perkin Elmer DSC 6000) and thermo gravimetric analysis (with Perkin Elmer TGA 4000) (Fig. 1a, b).

Data Collection and Structure Solution and Refinement

Single crystal X-ray diffraction data of both the crystals (**CHRM** and **CHRM·H$_2$O**) were collected on Bruker Smart APEX II diffractometer using MoKα (λ = 0.7107 Å). All the crystal structures were solved by direct methods using SIR 92 [43] and refined by the full matrix least squares method using SHELXL97 [44] present

Table 1 Crystallographic and refinement data

Data	CHRM	CHRM·H_2O
Molecular formula	$C_{10}H_8O_3$	$C_{10}H_8O_3.H_2O$
CCDC number	990313	990314
Molecular weight	176.16	194.18
Temperature (K)	298(2)	298(2)
Wavelength	0.71073	0.71073
Solvent system	Chloroform, 2-propanol	Acetone, THF, Acetonitrile
Crystal system	Orthorhombic	Monoclinic
Space group	$P2_12_12_1$	$P2_1/n$
a (Å)	5.2399(1)	7.1239(6)
b (Å)	11.8776(3)	11.3561(7)
c (Å)	13.1891(4)	11.8347(9)
α, β, γ (°)	90, 90, 90	90, 105.298(8), 90
Z/Volume (Å^3)/ρ (g/cm^3)	4/820.86(4)/1.425	4/923.50(12)/1.397
F (000)/μ (mm^{-1})	368/0.106	408/0.109
$\theta_{min,\ max}$	3.09, 24.99	2.53, 25.00
$h_{min,max}$;$k_{min,max}$; $l_{min,max}$	−5, 6; −14, 14; −15, 15	−8, 8; −13, 13; −14, 14
Treatment of hydrogens	Fixed	Mixed
No. of reflections.	3961	7647
No. unique/observedreflections.	1394, 1326	1628, 1088
No. of parameters	121	138
R_all, R_obs	0.0320, 0.0304	0.0736, 0.0443
wR_2_all, wR_2_obs	0.0843, 0.0830	0.1207, 0.0963
$\Delta\rho_{min,max}$ (eÅ^{-3})	−0.143, 0.133	−0.204, 0.158
GooF	1.089	1.090

in the program suite WinGX [45]. ORTEP of all the compounds were generated using ORTEP32 [46] and packing diagrams were generated using Mercury 3.0 [47]. Geometrical calculations were done using PARST [48] and PLATON [49].The non-hydrogen atoms are refined anisotropically and the hydrogen atoms bonded to C and O atoms were positioned geometrically and refined using a riding model with distance restraints of O–H = 0.82 Å, aromatic C–H = 0.95 Å, C(sp^3)–H = 0.98 and with $U_{iso}(H) = 1.2U_{eq}(C_{sp2})/1.5U_{eq}(O,C_{sp3})$. In case of **CHRM·$H_2O$**, the hydrogen atoms connected to water oxygen were located from the difference electron density map and refined with isotropic displacement parameter. Table 1 lists all crystallographic and refinement data. Intermolecular interactions are listed in Table 2.

Theoretical Calculations

The lattice energies of the coumarin derivatives (**CHRM**) and its hydrate (**CHRM·H_2O**) were calculated by CLP computer program package [version 10.2.2012] [50], the total energy being partitioned into their Coulombic, polarization, dispersion and repulsion contributions (Table 3). The selected molecular pairs along with their interactions energies (with the total interaction energy partitioned into their Coulombic, polarization, dispersion and repulsion contributions) were extracted from the crystal packing. These are presented in Table 2.

Hirshfeld Surfaces and Electrostatic Potentials

Hirshfeld surfaces mapped with different properties e.g. d_{norm}, shape index, curvedness etc. were generated using CrystalExplorer 3.0 [51]. These have proven to be a useful visualization tool for the analysis of intermolecular interactions and the crystal packing behaviour of molecules, particularly for the purpose of comparison of two or more solid forms of a given compound [52, 53]. The 2D-fingerprint plot was also generated which provides decomposition of the Hirshfeld surfaces into contributions from the different intermolecular interactions present in the crystal structure. It was of interest to analyze intermolecular interactions present in the crystal packing in terms of a visual study based on electrostatic complementarities. Therefore, the electrostatic potential (ESP) were also mapped on the Hirshfeld surface over the range −0.01 au (red), through 0 (white), to 0.01 au (blue) in this study [39]. For this purpose, ab initio wavefunctions were obtained with a MIDI! basis set at the Hartree–Fock level and the molecular geometries are taken directly from the relevant

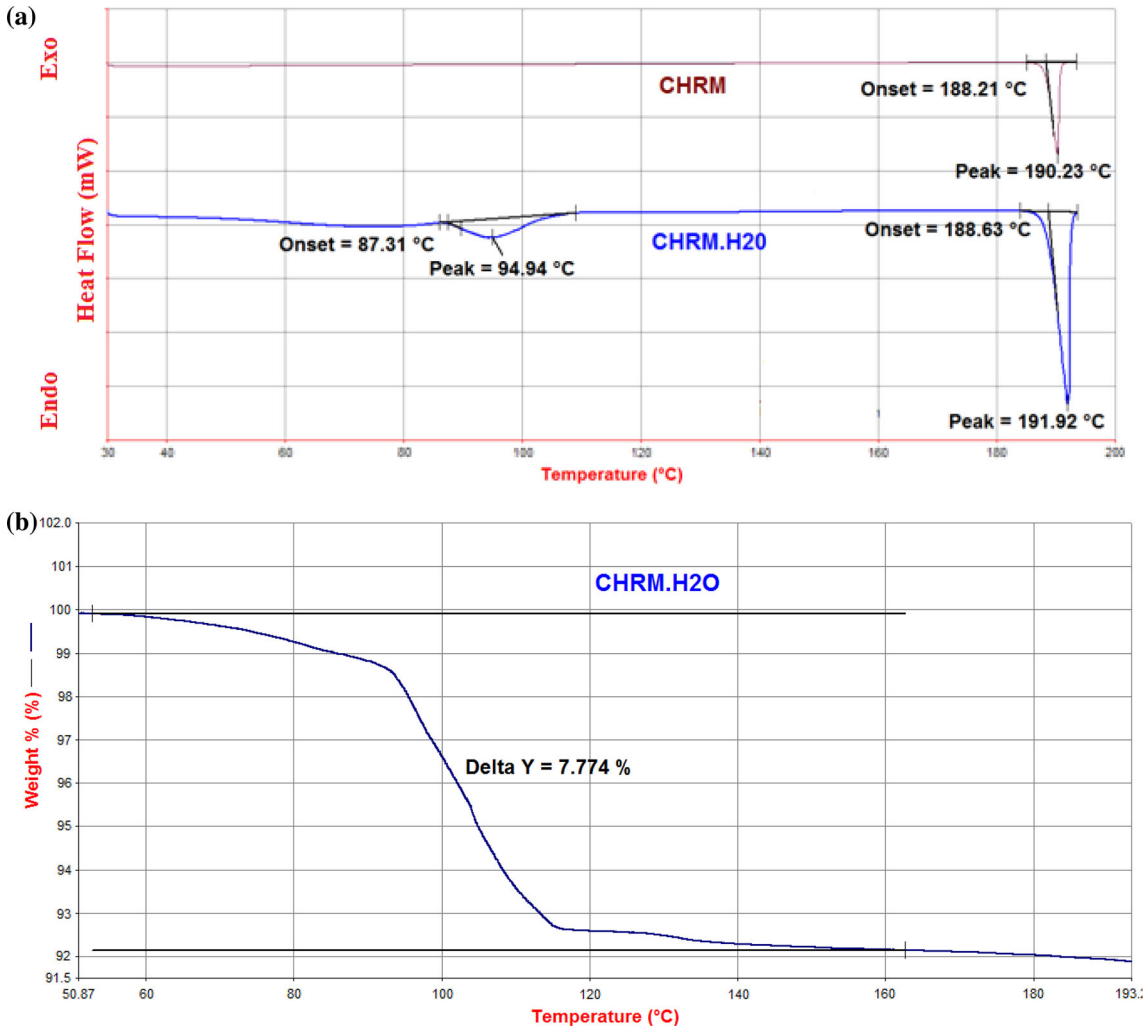

Fig. 1 **a** DSC plots for **CHRM** and **CHRM·H$_2$O**, **b** TGA plot of 7-hydroxy-4-methyl-2*H*-chromen-2-one hydrate (**CHRM·H$_2$O**)

crystal structures. The ESPs mapped on the Hirshfeld surfaces were also compared with ESPs mapped on 0.0004 au isosurface of the electron density for the isolated molecules at their solid state and optimized geometry. For this purpose, the electron density and the ESP were calculated by TURBOMOLE [54, 55] at DFT-D3/B97-D level of calculation using aug-cc-pVTZ basis set and the graphics were generated with gOpenMol 3.0 [56, 57]. The optimized geometry of an isolated molecule have been obtained by performing DFT calculations at the B3LYP/6-31G** using TURBOMOLE with crystallographic coordinates as the starting geometry.

Differential Scanning Calorimetry and Thermogravimetry Analysis

DSC measurements show that the loss of water occurs at 87.3 °C in case of the hydrate (**CHRM·H$_2$O**). Subsequently, both **CHRM** and **CHRM·H$_2$O** melt at the same temperature of 188 °C (Fig. 1). The experimental mass loss, 7.8 % in TGA analysis is comparable to the theoretically calculated value of 9.1 % for the loss of one molecule of water.

Results and Discussion

The *ORTEP* of 7-hydroxy-4-methyl-2*H*-chromen-2-one (**CHRM**) and its mono hydrate (**CHRM·H$_2$O**) with the corresponding atom numbering scheme are presented in Fig. 2. The water molecule in the asymmetric unit of **CHRM·H$_2$O** is connected via the formation of strong O–H···O$_{water}$ hydrogen bond. The molecular structure of the title compound reveals that it contains only one hydroxyl (−OH) group present as a strong hydrogen bond donor. The carbon atom in the ring (sp^2 hybridized) and the methyl carbon (sp^3 hybridized) atom can also act as weak hydrogen bond donors. The molecule contains the

Table 2 List of the intermolecular interactions along with the PIXEL interaction energies (I.E. in kcal/mol) between selected molecular pairs related by a symmetry operation

Motifs	D–X···A/D···A	D···A (Å)	X···A (Å)	∠D–X···A (°)	Symmetry	Centroid distance (Å)	E_{Cou}	E_{Pol}	E_{Disp}	E_{Rep}	E_{Tot}
CHRM ($P2_12_12_1$)											
I	O3−H3···O2=C9	2.714(2)	1.78	177	−x + 1/2, −y, z−1/2	8.543	−14.9	−6.2	−3.0	15.0	−9.2
	C2–H2···O2=C9	3.355(2)	2.61	125							
II	C8–H8···O2=C9	3.411(2)	2.37	161	x + 1/2, −y + 1/2, −z + 2	8.647	−2.7	−1.1	−2.6	2.6	−3.7
	C10–H10A···O2=C9	3.654(2)	2.66	152							
III	C5–H5···O3	3.517(2)	2.69	133	x + 1/2, −y + 1/2, −z + 1	6.478	−1.8	−0.8	−5.2	4.2	−3.6
	C5–H5···π(C3)	3.521(2)	2.79	125							
IV	C10–H10C···Cg1	3.833(2)	2.82	157	x + 1, y, z	5.240	−0.7	−1.1	−5.7	4.1	−3.4
V	C10–H10B···O1	3.794(2)	2.85	146	−x + 1, y + 1/2, −z + 3/2	6.280	−0.3	−0.8	−3.0	1.6	−2.5
VI	O3(*lp*)···C9=O2	3.715(2)	2.992(2)	112	−x + 3/2, −y, z−1/2	7.485	−1.0	−0.6	−2.9	2.4	−2.2
CHRM·H_2O ($P2_1/n$)											
I	O3–H3···O4 W	2.658(3)	1.73	171	x, y, z	5.309	−17.2	−7.6	−2.9	18.8	−9.0
	C2–H2···O4 W	3.421(3)	2.71	123							
II	O4 W–H4A···O2	2.883(3)	1.95	170	−x + 3/2, y−1/2, −z + 1/2	5.461	−8.7	−2.9	−1.9	7.5	−5.9
III	O4 W–H4B···O2	2.791(3)	1.86	172	x−1/2, −y + 1/2, z−1/2	6.207	−9.9	−3.7	−1.8	10.3	−5.1
IV	C5–H5···O3	3.369(3)	2.42	146	x + 1/2, −y−1/2, z + 1/2	7.752	−3.5	−0.6	−2.0	0.5	−5.5
V	π···π stacking (C2···Cg1)	3.396(2)	–	–	−x + 2, −y, −z + 1	3.578	−0.7	−1.2	−10.0	6.8	−5.2
	lp(O1)···Cg2	3.415(2)									
VI	π···π stacking (C2···Cg2)	3.360(2)	–	–	−x + 1, −y, −z + 1	4.546	−1.1	−0.7	−8.3	5.9	−4.3
	lp(O3)···Cg1	3.340(2)									

Cg1 and Cg2 are referred to the centre of gravity of the ring formed by O1–C1–C6–C7–C8–C9 and C1–C2–C3–C4–C5–C6 respectively

Table 3 Lattice energy calculation (kcal/mol) partitioned into Coulombic, polarization, dispersion and repulsion contributionwith PIXEL method in CLP program package

	Comp. Code	E_{Coul}	E_{Pol}	E_{Disp}	E_{Rep}	E_{Tot}
1.	**CHRM**	−23.0	−9.7	−25.2	30.5	−27.4
2.	**CHRM·H$_2$O**	−21.1	−9.0	−14.9	24.5	−20.6

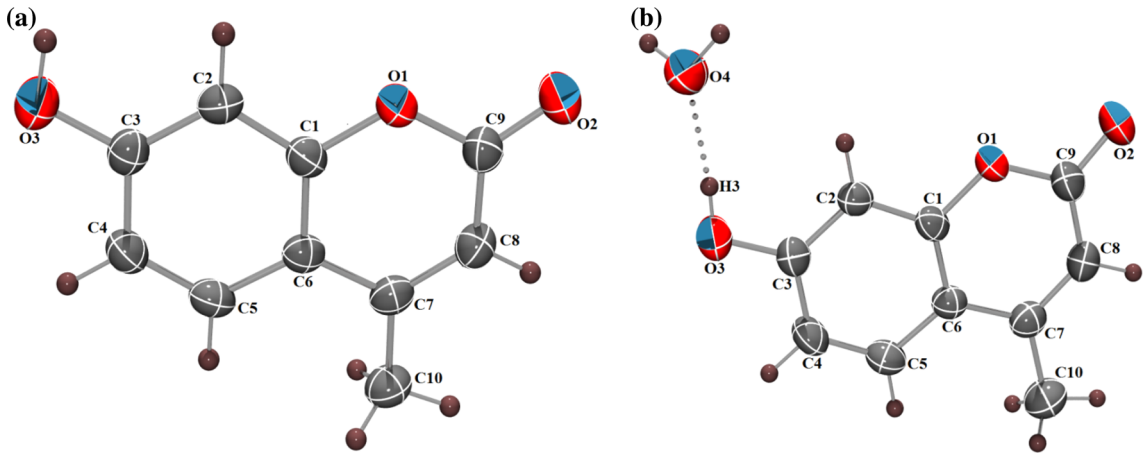

Fig. 2 *ORTEP* diagram of **a** 7-hydroxy-4-methyl-2*H*-chromen-2-one (**CHRM**) and **b** 7-hydroxy-4-methyl-2*H*-chromen-2-one hydrate (**CHRM·H$_2$O**) drawn at 50 % probability level

following set of strong hydrogen bonds with the different acceptor oxygen atoms: the first one is the carbonyl O-atom (O2), the second one is the hydroxyl oxygen (O3) and the third one is the ester O-atom (O1). Apart from these, the π-ring can also act as a weak hydrogen bond acceptor in both the cases. The inclusion of one water molecule in **CHRM·H$_2$O** introduces one strong hydrogen bond acceptor (having 2 *l.p.*) and two strong hydrogen bond donors. More ever, along with the possibility of formation of strong or weak hydrogen bonds, this molecule also has the potential to form weaker interactions such as π···π or *lp*···π in the crystal packing. The study of the nature of these weaker interactions is the main focus in this work in addition to the presence of strong hydrogen bonds.

Crystal Packing Analysis: Inputs from Interaction Energy and Lattice Energy Calculations by PIXEL Method

The compound **CHRM** crystallizes in the non-centrosymmetric orthorhombic space group $P2_12_12_1$ with Z = 4 (Fig. 2**a**). In the crystal packing of the compound, the strong O3–H3···O2 along with weak C2–H2···O2 hydrogen bonds (motif **I**, I.E. being −9.2 kcal/mol, Fig. 3a) utilizing 2_1 screw axis parallel to crystallographic *c*-axis direct the formation of a zigzag molecular ribbon (Fig. 3b, marked with pink coloured tape). Such ribbons are then interconnected with a similar stabilizing motif **II** (I.E = −3.7 kcal/mol) and motif **III** (I.E = −3.6 kcal/mol, Table 2). The motif **II** consists of a bifurcated weak C_{sp2}–H···O=C and C_{sp3}–H···O=C hydrogen bonds while a weak C_{sp2}–H···$O_{hydroxy}$ connects the molecules in motif **III** (Fig. 3a, b). It is to be noted that the packing of the molecules in **CHRM** shows the involvement of the $O_{hydroxy}$(*lp*)···C=O interactions (motif **VI**, I.E = −2.2 kcal/mol, Fig. 3a) which is involved in the formation of a molecular chain with the utilization of 2_1 screw axis along the crystallographic *c*-axis (Fig. 3b). The chain is then interconnected via the C_{sp3}–H···π (motif **IV**, I.E = −3.4 kcal/mol, Fig. 3a; Table 2) and the involvement of the motif **I**.

The hydrate of 7-hydroxy-4-methyl-2*H*-chromen-2-one (**CHRM·H$_2$O**) crystallizes in the centrosymmetric monoclinic $P2_1/n$ space group. In the asymmetric unit, one 7-hydroxy-4-methyl-2*H*-chromen-2-one molecule is found to be connected with one water molecule forming a strong hydrogen bond with the oxygen atom of the hydroxyl group acting as hydrogen bond donor (Fig. 2b) and observed to be the most stabilizing molecular motif (interaction energy being −9.0 kcal/mol)in the crystal packing (Fig. 4a). The crystal packing of **CHRM·H$_2$O** completely differs from **CHRM** with the presence of water molecule in the crystal. The molecules of 7-hydroxy-4-methyl-2*H*-chromen-2-one is interconnected with water molecules forming a 2D molecular layer down the *bc* plane

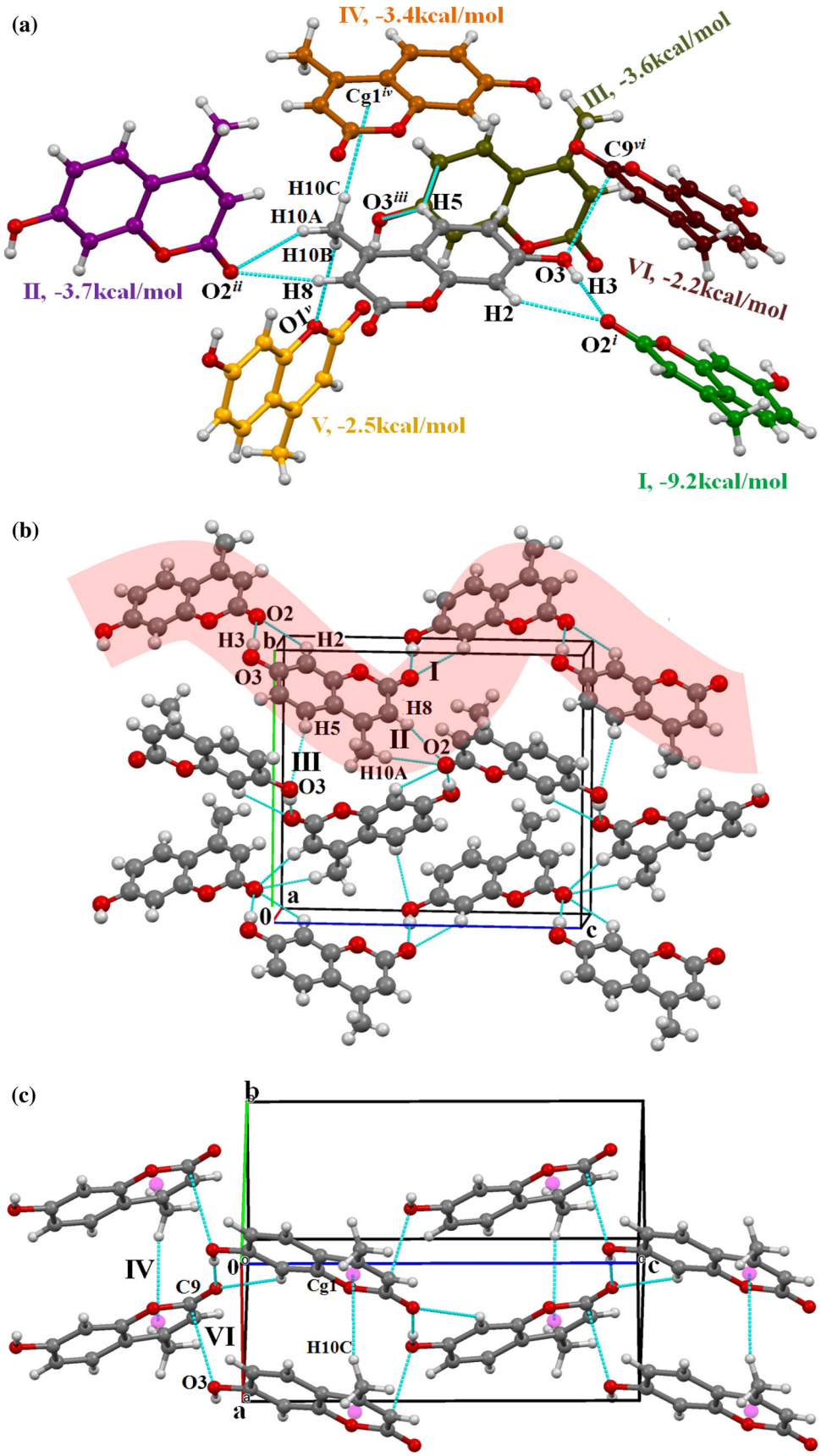

Fig. 3 **a** The coordination environment around the central molecule (C-atoms are grey, symmetry code: **x, y, z**) displaying the six structural motifs (C-atoms are in different colour for different molecules) in **CHRM** along with the intermolecular interactions which connects the central molecule with the neighbouring molecules (from Table 2). Symmetry codes being *i* − x + 1/2, −y, z−1/2; *ii* x + 1/2, −y + 1/2, −z + 2; *iii* x + 1/2, −y + 1/2, −z + 1; *iv* x + 1, y, z; *v* −x + 1, y + 1/2, −z + 3/2; *vi* −x + 3/2, −y, z−1/2. **b** Packing view down the *bc* plane in **CHRM** displaying strong O–H···O=C, weak C(sp^2)–H···O=C and C(sp^3)–H···O=C hydrogen bonds. **c** Packing of molecules in **CHRM** via the network of O(*lp*)···C=O, C(sp^3)–H···π along with strong O–H···O and weak C–H···O hydrogen bonds

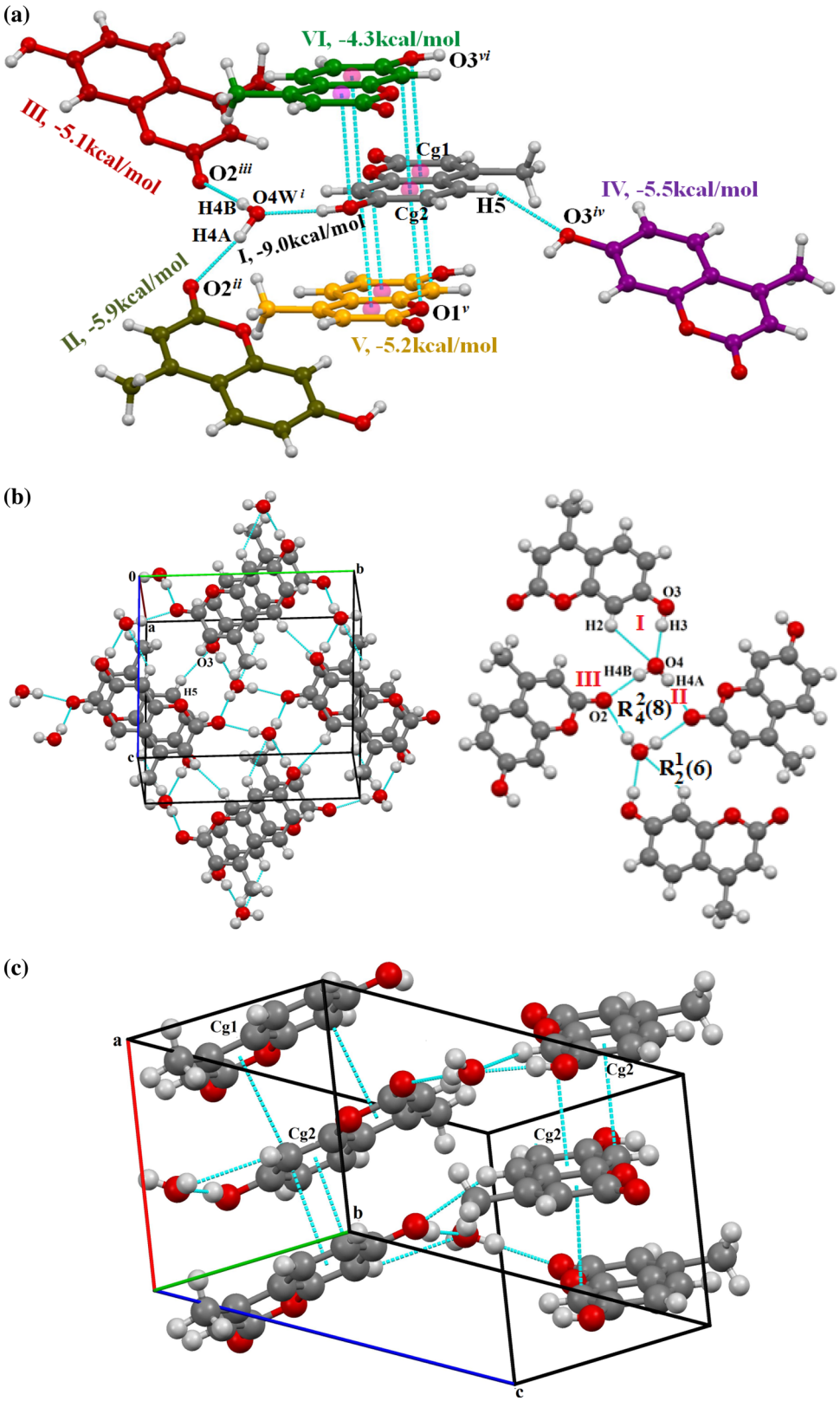

Fig. 4 **a** The coordination environment around the asymmetric unit in **CHRM·H$_2$O** (C-atoms are grey, symmetry code: **x, y, z**) displaying the six structural motifs (C-atoms are in different colour for different molecules) along with the intermolecular interactions which connects the central molecule with the neighbouring molecules (from Table 2). Symmetry codes being *i* x, y, z; *ii* −x + 3/2, y−1/2, −z + 1/2; *iii* x−1/2, −y + 1/2, z−1/2; *iv* x + 1/2, −y−1/2, z + 1/2; *v* −x + 2, −y, −z + 1; *vi* −x + 1, −y, −z + 1. **b** Packing view down the *bc* plane via strong O–H···O and weak C–H···O hydrogen bonds in **CHRM.H$_2$O** (*left*) and extracted packing motif displaying O–H···O hydrogen bonds that connects 7-hydroxy-4-methyl-2*H*-chromen-2-one molecules with water in **CHRM.H$_2$O** (*right*). **c** Crystal packing showing the presence of weak π···π interactions in the packing of molecules in **CHRM·H$_2$O**

(Fig. 4b). The four molecules of 7-hydroxy-4-methyl-2*H*-chromen-2-one and two molecules of water were found to be interconnected via $R_4^2(8)$ dimer and $R_2^1(6)$ [58, 59] hydrogen bond motifs (Fig. 4b). These were observed to involve molecular motifs **I**, **II** and **III** in the crystal packing (Table 2). The motif **I** (I.E = −9.0 kcal/mol) depicts

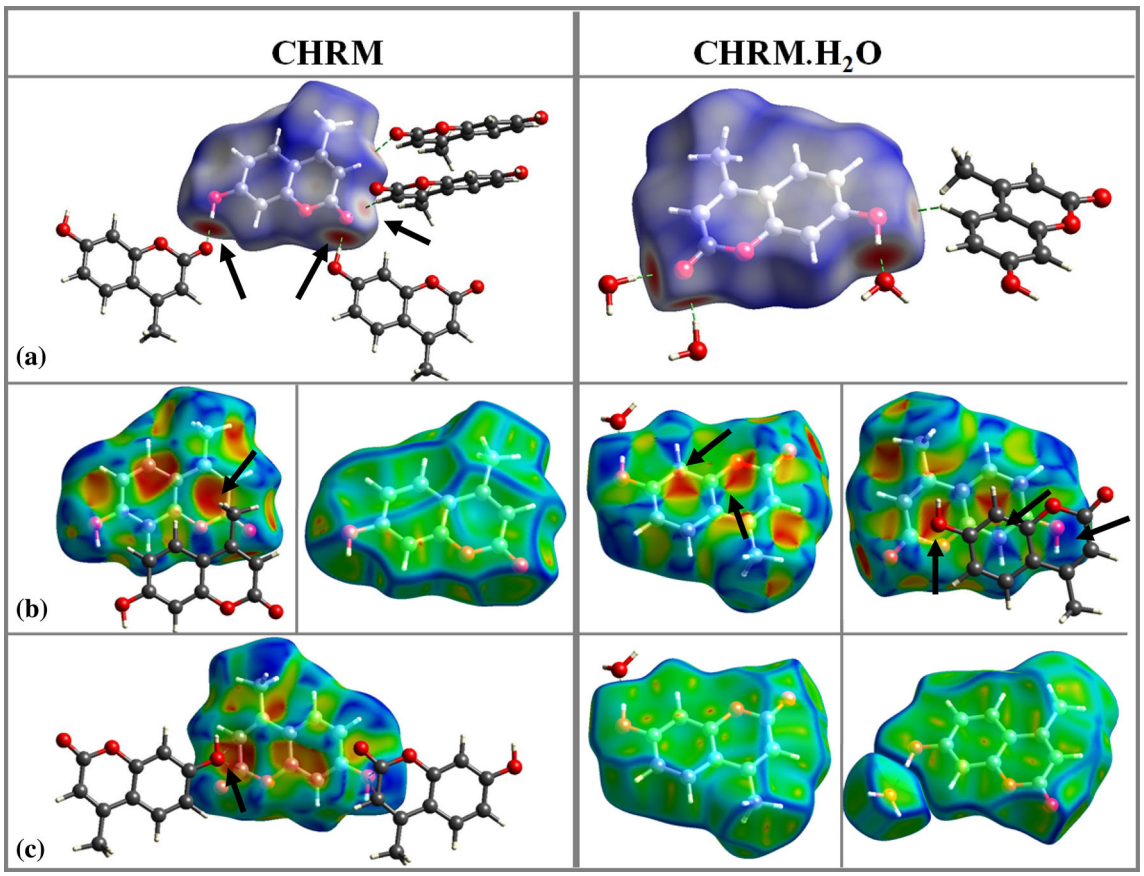

Fig. 5 **a** Hirshfeld surface mapped with d_{norm} of **CHRM** (*left column*) and **CHRM.H$_2$O** (*right column*) surrounded by a cluster of neighbouring molecules. **b**, **c** Hirshfeld surface mapped with shape index or curvedness of **CHRM** (*left column*) and **CHRM·H$_2$O** (*right column*)

strong O–H···O$_{water}$ along with the presence of weak C$_{sp2}$–H···O$_{water}$ hydrogen bonds while motif **II** (I.E = −5.9 kcal/mol) and motif **III** (I.E = −5.1 kcal/mol) displays the formation of a strong O$_{water}$–H···O=C hydrogen bond (Fig. 4a). Hence the O–H···O hydrogen bond with hydroxyl group oxygen acting as a donor and the carbonyl oxygen atom acting as an acceptor in **CHRM** is now replaced in the case of **CHRM.H$_2$O** with the oxygen atom of the water molecule acting both as an acceptor for the hydrogen atom from the hydroxyl group of the coumarin moiety and a hydrogen bond donor for the carbonyl oxygen in the crystal packing of **CHRM·H$_2$O**. The only common intermolecular interaction in **CHRM·H$_2$O** with **CHRM** is C5–H5···O$_{hydroxy}$[motif **IV**] and is found to contribute 5.5 kcal/mol towards the stabilization of the crystal packing (Fig. 4b). Furthermore, the crystal packing of **CHRM·H$_2$O** is stabilized by the presence of weak π···π stacking interactions (Motif **V** (I.E = −5.2 kcal/mol) and motif **VI** (I.E = −4.3 kcal/mol) (Fig. 4b, c) which are absent in the crystal packing of **CHRM**.

Lattice energy calculations for **CHRM** and **CHRM·H$_2$O** reveal that the major contribution towards the total lattice energy comes from the coulombic and dispersion energy term (Table 3). The anhydrous form (**CHRM**) is 6.8 kcal/mol more stable (Table 3) than the hydrate (**CHRM·H$_2$O**). This mainly arises due the difference in contribution from the dispersion energy in these. It is of interest to note that the contribution from dispersion energy in case of **CHRM** is 10.3 kcal/mol more than that in **CHRM·H$_2$O** (Table 3).

Analysis Hirshfeld Surfaces and Electrostatic Potentials

Hirshfeld surfaces mapped with different properties e.g. d_{norm}, shape index, curvedness have been proven to be a useful tool for the analysis of intermolecular interactions present in the crystal packing, particularly in comparing two different polymorphs (including solvates and hydrates) of a compound which may involve different intermolecular interactions in their crystal packing. Therefore it is of interest to analyze the dissimilarity present in the crystal packing of the anhydrous (**CHRM**) and hydrate (**CHRM·H$_2$O**) of the compound 7-hydroxy-4-methyl-2*H*-chromen-2-one by the Hirshfeld surfaces mapped with different properties (Fig. 5).

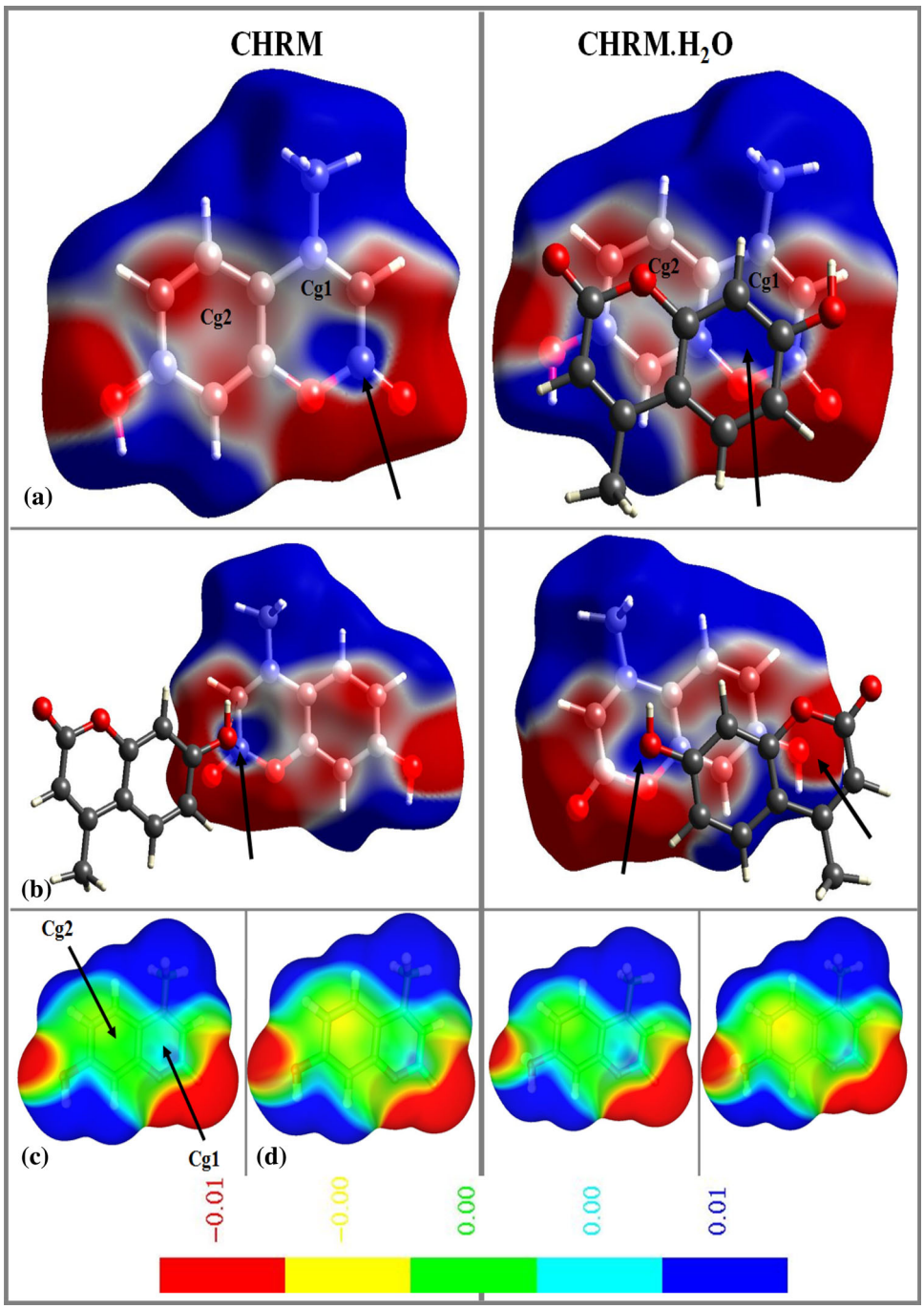

Fig. 6 Electrostatic potential mapped on the Hirshfeld surfaces of **CHRM** (*left column*) and **CHRM·H$_2$O** (*right column*) over the range −0.01 au (*red*) through 0.0 (*white*) to 0.01 au (*blue*) **a** front view and **b** back view. Electrostatic potential mapped on 0.0004 eÅ^{-3} isosurface over the range of −0.01au to 0.01 au calculated at DFT-D3 (B97-D)/aug-cc-pVTZ **c** at solid state geometry and **d** for isolated molecule for **CHRM**. The corresponding diagram for **CHRM·H$_2$O** is on the *right column*. (Color figure online)

The volume and the surface area of the Hirshfeld surface for **CHRM** and **CHRM·H$_2$O** were observed to be similar (200.35 Å^3/200.38 Å^2 vs. 201.36 Å^3/202.07 Å^2 for **CHRM** and **CHRM·H$_2$O** respectively). The red spots (corresponds to the contacts which appeared at less than the sum of the van der Waals radii) present on d_{norm} for **CHRM** and **CHRM·H$_2$O** correspond to the different molecular motifs in their crystal packing (Fig. 5a). The strong network of hydrogen bonds (**O3–H3···O2=C9**) in motif **I** of **CHRM** is reflected as the presence of the large red spot on the d_{norm} surface while small red dots over d_{norm} surface represent weak C8–H8···O2 (motif **II**, 2.37 Å, 161°, Table 2) hydrogen bonds (Fig. 5a, left column). It is to be noted that these corresponds to the first two most stabilizing intermolecular interactions in **CHRM** (Table 2). The presence of the big red spot over d_{norm} surfaces for **CHRM·H$_2$O** (Fig. 5a, right column) display the network of strong hydrogen bond between 7-hydroxy-4-methyl-2*H*-chromen-2-one molecule and water molecules in the crystal structure of **CHRM·H$_2$O**. The analysis

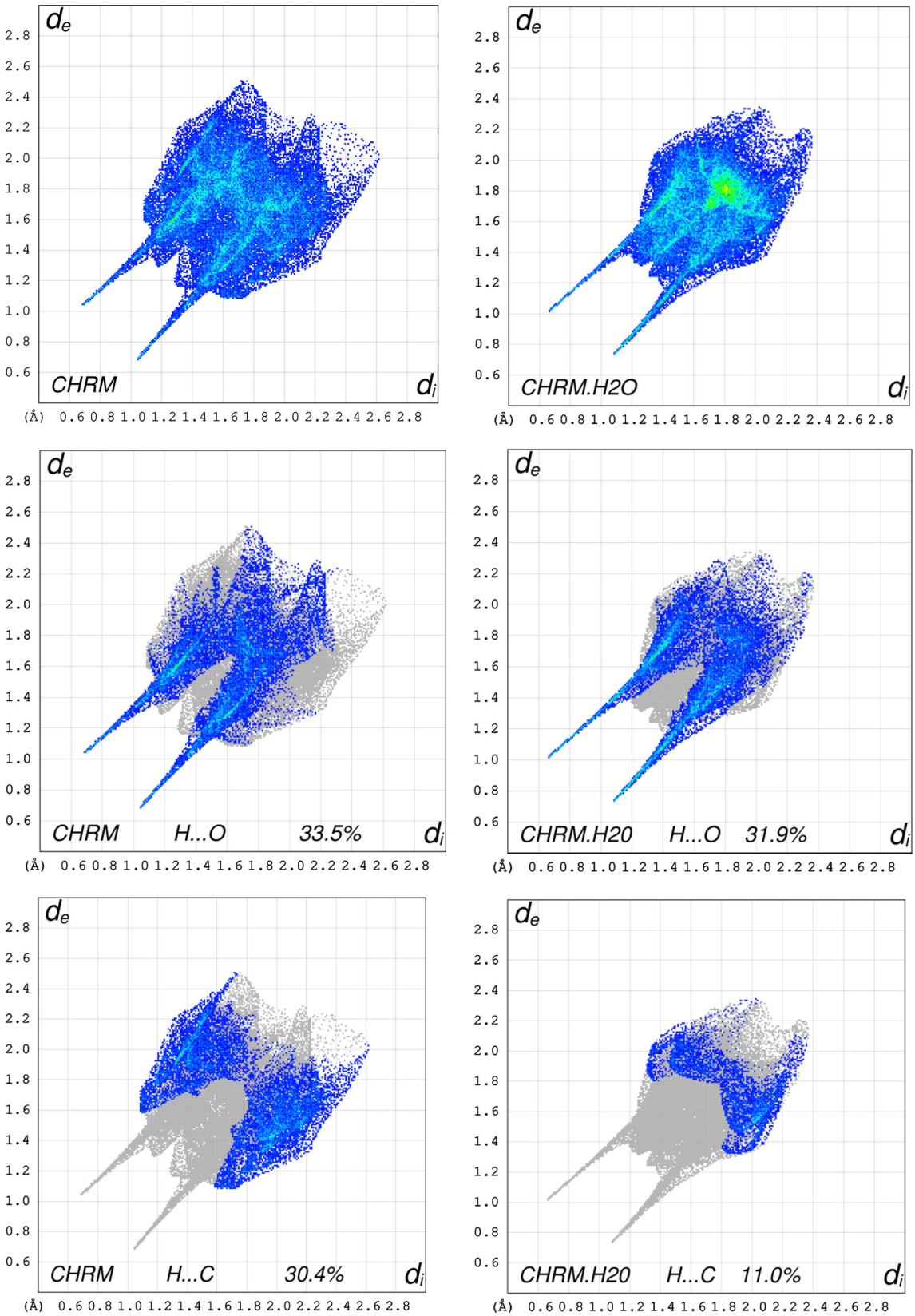

Fig. 7 2D fingerprint plots and its partition for different interactions for **CHRM** (*left column*) and **CHRM·H_2O** (*right column*)

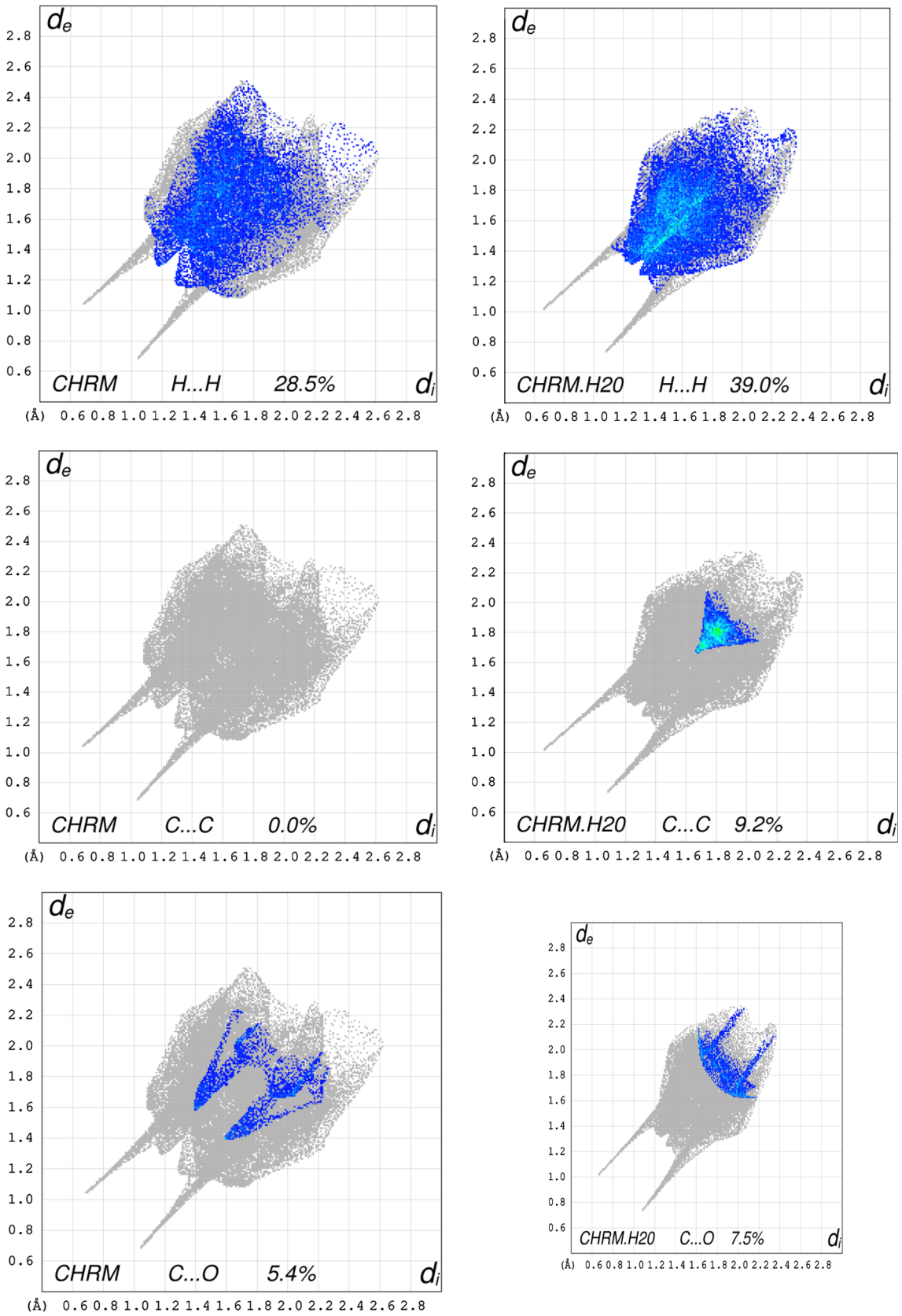

Fig. 7 continued

of the crystal packing revealed that the two crystal structures possessed the main differences in their crystal packing in term of weak interactions like C–H···π, *lp*···π, π ···π interactions.The Hirshfeld surface mapped with the properties shape index and curvedness were appropriate to analyze these interactions (Fig. 5b, c).The big red spot on Hirshfeld surface mapped with shape index appeared over the heterocyclic ring (Cg1, marked with arrow) of **CHRM** (Fig. 5b, left column) corresponds to the presence of C–H···π intermolecular interaction in the crystal structure. While the presence of adjacent red and blue triangles pairs (Fig. 5b), right column, marked with the arrows] on the shape index of **CHRM·H$_2$O** is a characteristic feature for the presence of π···π interactions in the crystal structure of **CHRM·H$_2$O.** Moreover curvedness surface of **CHRM·H$_2$O** shows broad and flat region over the molecular plane characteristics for the molecular stacking which is absent in case of **CHRM** (Fig. 5b, c).

To get a better understanding towards the presence of such weak interactions (*lp*···π, π···π) which stabilized the crystal packing, electrostatic potentials (ESP) were mapped over the Hirshfeld surfaces of **CHRM** and **CHRM·H$_2$O** (Fig. 6). It also allowed the visual study of electrostatic complementarities in the crystal packing. The main difference on the ESP (mapped over the Hirshfeld surfaces) of **CHRM** and **CHRM·H$_2$O** appeared over the Cg1 and Cg2 rings. It may explain the reason for the participation of different interactions by these rings in **CHRM** and **CHRM·H$_2$O** (Fig. 6, left and right columns for **CHRM** and **CHRM·H$_2$O**) respectively. The electropositive region above Cg1 ring is located over the carbonyl C-atom 'C9' in case of **CHRM** (Fig. 6a, left column) while the corresponding region (right column, marked with arrow) in case of **CHRM·H$_2$O** was found to be extended above the Cg1 ring. It is also observed in both the cases that there is an electronegative region over the Cg2 ring while the region above Cg1 is electropositive in nature. With these features, associated with the ESP in both cases, the formation of a O3(*lp*)···C9 = O2 (motif **VI**) is facilitated in case of **CHRM** as the electronegative region around the hydroxyl oxygen atom 'O3'was observed to be interacting with the electropositive region at carbonyl C-atom 'C9' (showing the electrostatic complementarities in the crystal packing) (Fig. 6b, left column) while the condition becomes more favourable for the two π···π stacking motifs in **CHRM·H$_2$O**. The first one (Fig. 6a, right column, motif **V**) involves the interaction of the electropositive region above Cg1 with the electronegative region above the Cg2 ring. A closer inspection of the ESP for the second case (Fig. 6b, left column, for motif **VI**) reveals the interaction of the electronegative region around the hydroxyl oxygen atom 'O3' with the electropositive region over Cg1 ring, a possible case of *lp*···π interaction.

Furthermore, the electrostatic potential mapped on the Hirshfeld surfaces of **CHRM** (left column) and **CHRM·H$_2$O** (right column) were also compared with ESP mapped on the 0.0004 au isosurface at DFT-D3 (B97-D)/aug-cc-pVTZ at both the solid state geometry (Fig. 6c) and for the optimized [at DFT (B3-LYP)/6-31G**] isolated molecule(Fig. 6d) and these appear to be similar in both **CHRM** and **CHRM·H$_2$O**. The Cg1 ring was found to be more electropositive than Cg2 in the ESP mapped at the solid state geometry (for both **CHRM** and **CHRM·H$_2$O**, Fig. 6c). This phenomenon is less prominent at ESP for the optimized isolated molecule. Finally, an electropositive region was also observed above the carbonyl C-atom in both cases.

Fingerprint Plot Analysis

The comparisons of the 2D fingerprint plots (Fig. 7) reflect that these are distinctly different and hence reflect different packing motifs and intermolecular interactions in the two cases. The plot for the **CHRM·H$_2$O** appeared to be more compact than that of **CHRM**. The relative contributions due to strong O–H···O hydrogen bond, appearing as pair of sharp spikes, over the Hirshfeld surface of the molecule are similar in both (33.5 % in case of **CHRM** while 31.9 % in case of **CHRM·H$_2$O**). The main difference comes from the contribution of weak interactions. The H···C contacts (C–H···π), appears as wings in the fingerprint plot, comprises 30.4 % of the surface area in **CHRM** with the closest contacts at approx 2.7 Å whereas in case of the hydrate it is only 11 % with the closest contact at approx 3.1 Å. More ever, there is 9.2 % contribution coming from C···C contacts (π···π) with the closest at approximately 3.4 Å in case of the hydrate, while no contribution from C···C contacts in case of anhydrous form. This actually reflects the presence of the weak C–H···π hydrogen bond only in **CHRM** while **CHRM·H$_2$O** consist of π···π interactions which was found to be absent in the anhydrous form. It is to be also noted that the finger print plot for C···O interaction in **CHRM** appears as a long spike (around $d_e = 1.40$ and $d_i = 1.60$) hence suggesting it is may be due to the presence of O(*lp*)···π interactions in **CHRM**. Furthermore, contribution from the H···H contacts were observed to be the highest towards the Hirshfeld surfaces, the contribution being 39 and 28 % in case of the hydrate and anhydrous form respectively.

Conclusions

The comparative analysis of the crystal packing of the coumarin derivatives and its hydrates with inputs from lattice energy and interaction energy calculations of

different intermolecular interactions revealed the presence of significant stabilization from weak interactions like C–H···O, C–H···π, π···π, *lp*···π etc. towards the crystal packing in the presence of strong O–H···O hydrogen bond. The interaction energy was observed in the decreasing order of stabilization as follows: O–H···O > C–H···O > π···π > C–H···π > *lp*···π. The analysis of electrostatic potential and the Hirshfeld surfaces mapped with different properties are very promising visualization tools in the study of the nature of intermolecular interactions between molecular pairs in the crystal packing. The two crystal structures were observed to be differed in terms of the presence of different weak intermolecular interactions. The weak C–H···π, O(*lp*)···C=O interactions were observed in the crystal packing of the anhydrous form while the π···π, O(*lp*)···π interactions appears to stabilize the crystal packing in case of its hydrate.

Thus we have established that this approach can be applied to different classes of molecules, forming polymorphs and a quantitative analysis of the crystal packing, enables an improved understanding of the origin of the differences which exist in crystal formation.

Acknowledgements PP thanks UGC-India for research scholarship. PP and DC acknowledge IISER Bhopal for research facilities and infrastructure. DC thanks DST-Fast Track Scheme for research funding. KNV thanks NRF South Africa for DST/NRF Innovation Postdoctoral Fellowship. BO and KNV acknowledge DUT South Africa for facilities and encouragement.

References

1. Yadav VR, Prasad S, Gupta SC, Sung B, Phatak SS, Zhang S, Aggarwal BB (2012) 3-Formylchromone interacts with cysteine 38 in p65 protein and with cysteine 179 in IκBα kinase, leading to down-regulation of nuclear factor-κB (NF-κB)-regulated gene products and sensitization of tumor cells. J Biol Chem 287(1):245–256
2. Lin CM, Huang ST, Lee FW, Kuo HS, Lin MH (2006) 6-Acyl-4-aryl/alkyl-5,7-dihydroxycoumarins as anti-inflammatory agents. Bioorg Med Chem 14:4402–4409
3. Sharma SD, Rajor HK, Chopra S, Sharma RK (2005) Studies on structure activity relationship of some dihydroxy-4-methylcoumarin antioxidants based on their interaction with Fe(III) and ADP. Biometals 18:143–154
4. Pawar RB, Mulwad VV (2004) Synthesis of some biologically active pyrazole, thiazolidine and azetidinone derivatives. Chem Heterocycl Comp 440:257–264
5. Rajski SR, Williams RM (1998) DNA cross-linking agents as antitumor drugs. Chem Rev 98:2723–2796
6. Valenti P, Fabbri G, Rampa A, Bisi A, Gobbi S, Da Re P, Carrara M, Sgevano A, Cima L (1996) Synthesis and antitumor activity of some analogues of flavone acetic acid. Anti-cancer Drug Des 11:243–252
7. Rollinger JM, Hornick A, Langer T, Stuppner H, Prast H (2004) Acetylcholinesterase inhibitory activity of scopolin and scopoletin discovered by virtual screening of natural products. J Med Chem 47:6248–6254
8. Shim YS, Kim KC, Chi DY, Lee KH, Cho H (2003) Formylchromone derivatives as a novel class of protein tyrosine phosphatase 1B inhibitors. Bioorg Med Chem Lett 13:2561–2563
9. Brühlmann C, Ooms F, Carrupt P-A, Testa B, Catto M, Leonetti F, Altomare C, Carotti A (2001) Coumarins derivatives as dual inhibitors of acetylcholinesterase and monoamine oxidase. J Med Chem 44:3195–3198
10. Zhang YY, Meng XM, Wang XL, Xu LH (2003) Studies on the synthesis and spectra characteristics of stilbenylcoumarin organic materials. Dyes Pigm 56:189–194
11. Seth SK, Sarkar D, Kar T (2011) Use of π–π forces to steer the assembly of chromone derivatives into hydrogen bonded supramolecular layers: crystal structures and Hirshfeld surface analyses. CrystEngComm 13:4528–4535
12. Seth SK, Sarkar D, Jana AD, Kar T (2011) On the possibility of tuning molecular edges to direct supramolecular self-assembly in coumarin derivatives through cooperative weak forces: crystallographic and Hirshfeld surface analyses. Cryst Growth Des 11:4837–4849
13. Munshi P, Jelsch C, Hathwar VR, Guru Row TN (2010) Experimental and theoretical charge density analysis of polymorphic structures: the case of coumarin 314 dye. Cryst Growth Des 10:1516–1526
14. Konovalova IS, Shishkina SV, Paponov BV, Shishkin OV (2010) Analysis of the crystal structure of two polymorphic modifications of 3, 4-diamino-1, 2, 4-triazole based on the energy of the intermolecular interactions. CrystEngComm 12:909–916
15. Bernstein J (2002) Polymorphism in molecular crystals. Oxford University Press, Oxford
16. Price SL (2009) Computed crystal energy landscapes for understanding and predicting organic crystal structures and polymorphism. Acc Chem Res 42(1):117–126
17. Price SL (2004) Quantifying intermolecular interactions and their use in computational crystal structure prediction. CrystEngComm 6:344–353
18. Nangia A, Desiraju GR (1998) In design of organic solids. Springer, Berlin
19. Desiraju GR (2011) A bond by any other name. Angew Chem Int Ed 50:52–59
20. Desiraju GR, Steiner T (1999) The weak hydrogen bond in structural chemistry and biology. Oxford University Press, Oxford
21. Martinez CR, Iverson BL (2012) Rethinking the term ''pi-stacking''. Chem Sci 3:2191–2201
22. Bloom JWG, Wheeler SE (2011) Taking the aromaticity out of aromatic interactions. Angew Chem Int Ed 123:7993–7995
23. Salonen LM, Ellermann M, Diederich F (2011) Aromatic rings in chemical and biological recognition: energetics and structures. Angew Chem Int Ed 50:4808–4842
24. Munshi P (2005) Ph. D. Thesis, Indian Institute of Science, Bangalore
25. Egli M, Sarkhel S (2007) Lone pair-aromatic interactions: to stabilize or not to stabilize. Acc Chem Res 40:197–205
26. Dawson RE, Hennig A, Weimann DP, Emery D, Ravikumar V, Montenegro J, Takeuchi T, Gabutti S, Mayor M, Mareda J, Schalley CA, Matile S (2010) Experimental evidence for the functional relevance of anion-pi interactions. Nat Chem 2:533–538
27. Robertazzi A, Krull F, Knapp EW, Gamez P (2011) Recent advances in anion–π interactions. CrystEngComm 13:3293–3300
28. Estarellas C, Frontera A, Quiñonero D, Deyà PM (2011) Anion-π interactions in flavoproteins. Chem Asian J 6(9):2316–2318
29. Shukla R, Mohan TP, Vishalakshi B, Chopra D (2014) Experimental and theoretical analysis of lp···π intermolecular

interactions in derivatives of 1,2,4-triazoles. CrystEngComm 16(9):1702–1713
30. Panini P, Mohan TP, Gangwar U, Sankolli R, Chopra D (2013) Quantitative crystal structure analysis of 1,3,4-thiadiazole derivatives. CrystEngComm 15:4549–4564
31. Panini P, Chopra D (2013) Quantitative insights into energy contributions of intermolecular interactions in fluorine and trifluoromethyl substituted isomeric N-phenylacetamides and N-methylbenzamides. CrystEngComm 15:3711–3733
32. Dunitz JD, Gavezzotti A (2005) Toward a quantitative description of crystal packing in terms of molecular pairs: application to the hexamorphic crystal system, 5-Methyl-2-[(2-nitrophenyl)amino]-3-thiophenecarbonitrile. Cryst Growth Des 5:2180–2189
33. Gavezzotti A (2003) Towards a realistic model for the quantitative evaluation of intermolecular potentials and for the rationalization of organic crystal structures Part I Philosophy. CrystEngComm 5:429–438
34. Gavezzotti A (2003) Towards a realistic model for the quantitative evaluation of intermolecular potentials and for the rationalization of organic crystal structures Part II Crystal energy landscapes. CrystEngComm 5:439–446
35. Dunitz JD, Gavezzotti A (2009) How molecules stick together in organic crystals: weak intermolecular interactions. Chem Soc Rev 38:2622–2633
36. Gavezzotti A (2003) Calculation of intermolecular interaction energies by direct numerical integration over electron densities. 2. An improved polarization model and the evaluation of dispersion and repulsion energies. J Phys Chem B 107:2344–2353
37. Spackman MA, Jayatilaka D (2009) Hirshfeld surface analysis. CrystEngComm 11:19–32
38. Spackman MA, McKinnon JJ (2007) Towards quantitative analysis of intermolecular interactions with Hirshfeld surfaces. Chem Commun:3814–3816
39. Spackman MA, McKinnon JJ, Jayatilaka D (2008) Electrostatic potentials mapped on Hirshfeld surfaces provide direct insight into intermolecular interactions in crystals. CrystEngComm 10:377–388
40. Vogel AI (1986) Vogel's textbook of practical organic chemistry, 4th edn. Pearson edu. Ltd, London, p 925
41. Yang S-P, Han L-J, Wang D-Q, Xia H-T (2007) Redetermination of 7-hydroxy-4-methyl-2*H*-1-benzopyran-2-one. Acta Cryst E 63:o4643
42. Butcher RJ, Jasinski JP, Yathirajan HS, Narayana B, Samshad (2007) 7-Hydroxy-4-methyl-2*H*-chromen-2-one monohydrate. Acta Cryst E63:o3412–o3413
43. Altomare A, Cascarano G, Giacovazzo C, Guagliardi A (1993) Completion and refinement of crystal structures with *SIR*92. J Appl Crystallogr 26:343–350
44. Sheldrick GM (2008) A short history of SHELX. Acta Crystallogr A64:112–122
45. Farrugia LJ (1999) WinGx suite for small-molecule single-crystal crystallography. J Appl Crystallogr 32:837–838
46. Farrugia LJ (1997) Ortep-3 for windows. J Appl Crystallogr 30:565–566
47. Macrae CF, Bruno IJ, Chisholm JA, Edgington PR, McCabe P, Pidcock E, Rodriguez-Monge L, Taylor R, Streek, J, Wood PA (2008) Mercury CSD 2.0—new features for the visualization and investigation of crystal structures. J Appl Crystallogr 41:466–470. www.ccdc.cam.ac.uk/mercury
48. Nardelli M (1995) *PARST*95—an update to *PARST*: a system of Fortran routines for calculating molecular structure parameters from the results of crystal structure analyses. J Appl Crystallogr 28:659
49. Spek AL (2009) Structure validation in chemical crystallography. Acta Crystallogr D65:148–155
50. Gavezzotti A (2011) Efficient computer modeling of organic materials. The atom–atom, Coulomb–London–Pauli (AA-CLP) model for intermolecular electrostatic-polarization, dispersion and repulsion energies. New J Chem 35:1360–1368
51. Wolff SK, Grimwood DJ, McKinnon JJ, Turner MJ, Jayatilaka D, Spackman MA (2012) CrystalExplorer (Version 3.0),University of Western Australia
52. McKinnon JJ, Spackman MA, Mitchell AS (2004) Novel tools for visualizing and exploring intermolecular interactions in molecular crystals. Acta Crystallogr B60:627–668
53. McKinnon JJ, Fabbiani FPA, Spackman MA (2007) Comparison of polymorphic molecular crystal structures through Hirshfeld surface analysis. Cryst Growth Des 7:755–769
54. Ahlrichs R, Baer M, Haeser M, Horn H, Koelmel C (1989) Electronic structure calculations on workstation computers: the program system TURBOMOLE. Chem Phys Lett 162:165–169
55. TURBOMOLE V6.3 2011, a development of University of Karlsruhe and Forschungszentrum Karlsruhe GmbH, 1989–2007, TURBOMOLE GmbH, since 2007. Available from http://www.turbomole.com
56. Bergman DL, Laaksonen L, Laaksonen A (1997) Visualization of solvation structures in liquid mixtures. J Mol Gr Modelling 15:301
57. Laaksonen L (2004) gOpenMol, version 3.00 Center of Scientific Computing, Espoo, Finland. http://laaksonen.csc.fi/gopenmol/
58. Etter MC (1991) Hydrogen bond as design element. J Phy Chem 95:4601–4610
59. Etter MC (1990) Encoding and decoding hydrogen bond patterns of organic compounds. Acc Chem Res 23:120–126